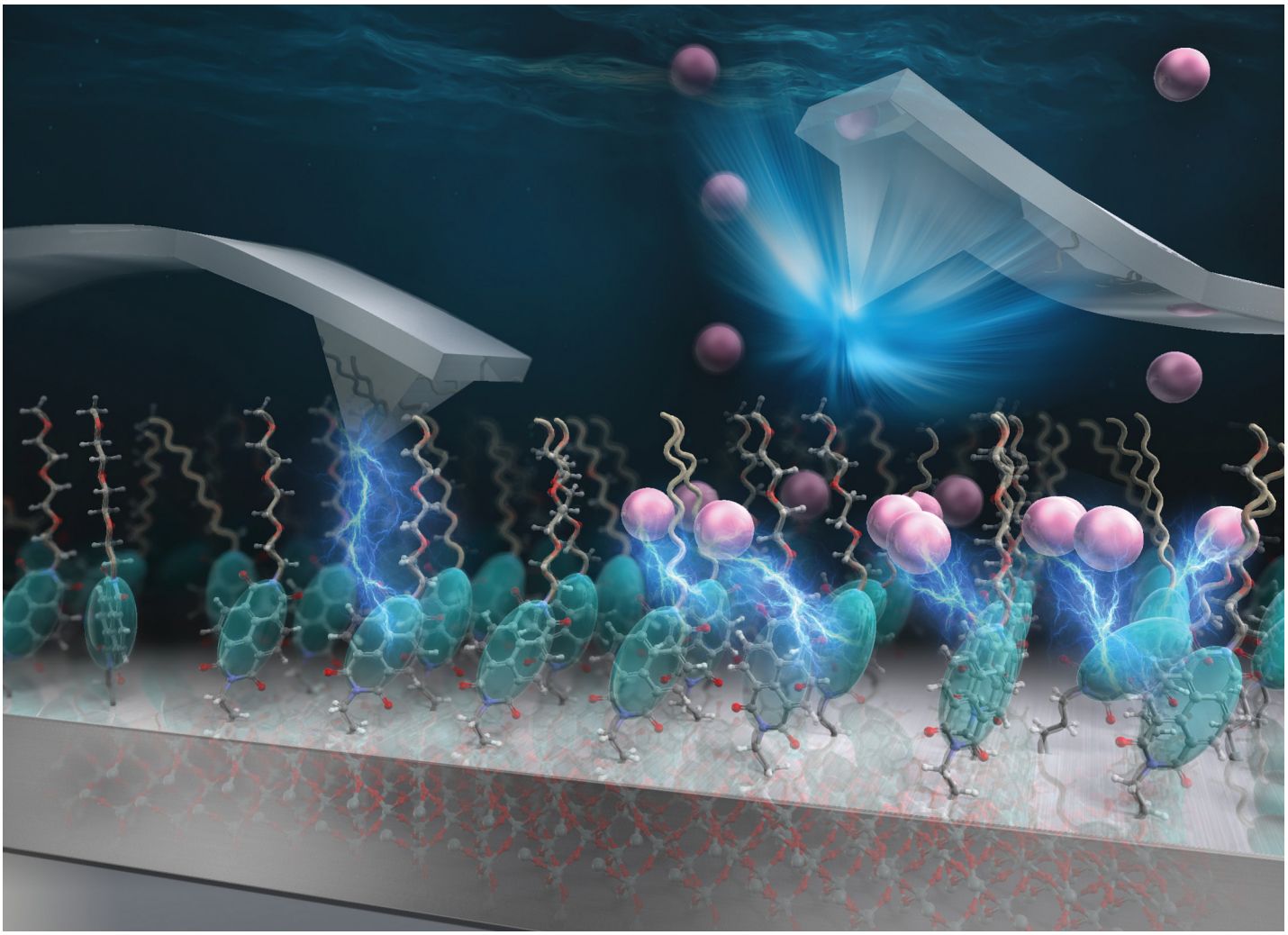

Showcasing research from Dr Masaaki Akamatsu's laboratory, Department of Pure and Applied Chemistry, Faculty of Science and Technology, Tokyo University of Science, Chiba, Japan.

Anion–π interaction at the solid/water interfaces

We report evaluations of the anion–π interactions at the solid/water interface. Force curve measurements revealed that a single-molecule force of anion–π interaction between a naphthalenediimide (NDI) unit and a negatively charged surface of the cantilever was ~40 pN.

As featured in:

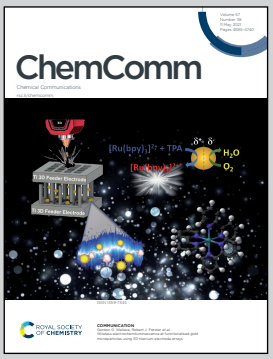

See Masaaki Akamatsu, Hideki Sakai *et al.*, *Chem. Commun.*, 2021, **57**, 4650.

ROYAL SOCIETY OF CHEMISTRY

rsc.li/chemcomm

Registered charity number: 207890

ChemComm

COMMUNICATION

View Article Online
View Journal | View Issue

Cite this: *Chem. Commun.*, 2021, **57**, 4650

Received 4th March 2021,
Accepted 9th April 2021

DOI: 10.1039/d1cc01186c

rsc.li/chemcomm

Anion–π interaction at the solid/water interfaces†

Masaaki Akamatsu, *[ab] Ayumi Kimura,[a] Koji Yamanaga,[a] Kenichi Sakai [ab] and Hideki Sakai*[ab]

Anion–π interaction has been found to play a key role in interfacial phenomena. In this study, we evaluated the anion–π interactions at the solid/water interface. Anion adsorption originating from anion–π interaction at the interfaces followed the hydration energy and the presence of conjugated systems of the anions by the QCM measurements. Force curve measurements revealed that the single-molecule force of anion–π interaction between an NDI unit and the negatively charged surface of the cantilever was ~40 pN. To the best of our knowledge, this is the first example of obtaining a single-molecule force for anion–π interactions.

Interfacial phenomena, such as wettability, friction, adhesiveness, and dispersion of colloidal particles, are important factors in determining material characteristics. The interfacial properties are mainly governed by physicochemical properties such as charge, hydrophilic–lipophilic balance, and surface morphology. Adsorption at solid/liquid interfaces, based on intermolecular interactions, has a significant impact on the interfacial properties. For example, amphiphilic molecules reversibly adsorb at the solid/liquid interface *via* electrostatic or hydrophobic interactions and contribute to the control of friction and colloidal dispersibility.

Intermolecular interactions arising in bulk water are inhibited because noncovalent bonds, based on electrostatic interactions, compete with solvation (hydration).[1] On the other hand, it is known that molecular interactions are enhanced at the interfaces in comparison to the bulk media[2–4] because the dielectric constant of water near the interface, such as the solid/water interface, is lower than that of the bulk water owing to the weakened dipole of aligned water molecules at the interface.[5] Therefore, the solid/water interface is a suitable space for intermolecular interactions and molecular recognition.

Anion–π interactions are noncovalent interactions between an electron-deficient aromatic ring and anion species.[1,6] When a strong electron-withdrawing group is introduced into an aromatic system, the charge distribution on the aromatic plane is inverted, whose negative quadrupole moment (Q_{zz}) then attracts anions.[1] Naphthalenediimide (NDI) bearing Q_{zz} of 18 B is an excellent acceptor for anion–π interactions. On the other hand, electron-rich aromatic compounds such as benzene attract cation species by comparable cation–π interactions.[7] Although anion–π interactions have been proposed by theoretical investigations, they have recently been observed in crystal structures and solutions[1,8–11] and have contributed to functional molecular systems.[12–14] Matile *et al.* reported the transport of anions across biological membranes[15] and in chemo- or enantioselective catalysis.[16] Simultaneously, it was revealed that many protein folding structures and enzymatic reactions are based on anion–π interactions.[17,18] Furthermore, Zeng *et al.* revealed that anion–π and cation–π interactions coexist during bioadhesion based on catecholic moieties with phosphate ester and potassium.[19] These reports reveal that anion–π interaction is an excellent tool to control not only small molecular functions but also macromolecular and macroscale phenomena at the material interfaces.

The nanomechanics of the molecular interactions were examined by force measurements using a surface force apparatus (SFA) or atomic force microscopy (AFM). Auletta *et al.* demonstrated the force measurements of the host–guest interaction of β-cyclodextrin monolayers on Au(111) with several guests immobilised on the AFM cantilever and evaluated the binding strength of the complexes.[20] Israelachvili characterised cation–π interactions in the adhesion proteins of marine organisms in aqueous media by force analysis and observed that the interactions play a key role in the underwater adhesion of marine creatures, such as mussels.[21] As mentioned above, anion–π interactions were also found to contribute to the biological adhesion process (SFA measurements).[22] Inhibition experiments with these anions have revealed that the strength of anion–π interactions follows the order $HPO_4^{2-} > SO_4^{2-} > NO_3^-$.

[a] *Department of Pure and Applied Chemistry, Faculty of Science and Technology, Tokyo University of Science, 2641 Yamazaki, Noda, Chiba, 278-8510, Japan*
[b] *Research Institute for Science and Technology, Tokyo University of Science, 2641 Yamazaki, Noda, Chiba, 278-8510, Japan*

† Electronic supplementary information (ESI) available. See DOI: 10.1039/d1cc01186c

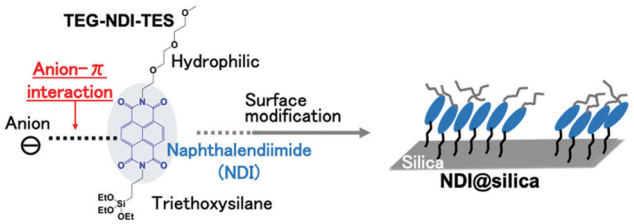

Fig. 1 Chemical structure of **TEG-NDI-TES** and immobilization on the silica substrate.

This trend is associated with the charge density, polarity, and hydration behaviour of the anions. This report demonstrated that interfacial analytical techniques have started to reveal anion–π interactions at the solid/water interfaces and their contributions to interfacial phenomena. This is the only report on anion–π interactions at interfaces. However, the system was investigated using complex biological molecules. For understanding the interaction at the interface, the system needs to be simplified.

To examine anion–π interactions at the solid/liquid interface, we immobilised an NDI derivative (**TEG-NDI-TES**; TEG: triethylene glycol) composed of an NDI core as a popular and simple anion–π acceptor and an alkoxysilyl group capable of covalent bonding with the silica surface (Fig. 1). Quartz crystal microbalance with dissipation (QCM-D) measurements revealed anion-binding of **NDI@silica**, based on anion–π interactions. At **NDI@silica**, we directly observed anion–π interactions and evaluated single molecular force by force curve measurements in water using AFM.

To evaluate anion–π interactions at the solid/water interface, we synthesised a new NDI derivative (**TEG-NDI-TES**), as shown in Scheme S1 (ESI†). For immobilisation, a silica substrate was immersed in a dichloromethane solution of **TEG-NDI-TES** (1.0 mM) for 15 h and then heated for 1 h at 100 °C to achieve film formation through the silane coupling reaction. After this modification, the Raman spectrum of **NDI@silica** was obtained. It showed characteristic bands of NDI derivatives, for example, 2901 (ν_s C–H), 2862 (ν_s C–H), and 1564 (ν_s/ν_{as} C=C) cm^{-1} (Fig. 2), which revealed the successful film formation of **TEG-NDI-TES**. The contact angle of **NDI@silica** with pure water was 61°, which is larger than that of the bare silica substrate, which also showed that an organic film was formed on the silica substrate (Fig. S3, ESI†). Furthermore, in the AFM phase image of **NDI@silica**, a rough surface morphology was observed, whereas the surface of the bare silica substrate was smooth (Fig. S4a, ESI†). The signal intensity in the AFM phase images represents the relative rheological properties of the surface. The **NDI@silica** image indicated that a soft organic film was formed on the hard silica substrate. These results confirmed that **TEG-NDI-TES** was successfully immobilised on the silica substrate.

Next, anion–π interactions between the NDI moieties on the substrate and anion species in THF were evaluated by a spectroscopic method. The UV/Vis absorption spectra of the **TEG-NDI-TES**-modified quartz substrate were measured in THF (Fig. S4b, ESI†). In the absence of anion species, characteristic bands of the NDI moiety were observed at 358 nm and 378 nm, originating from the 0–0 and 0–1 vibronic transitions, respectively.[23] With titration of fluoride anions with tetra-*n*-butylammonium fluoride (TBAF), the intensities of these bands decreased and the baseline around 400–600 nm increased. The absorption bands at 476 and 560 nm, originating from the NDI^- and NDI^{2-} radical anions, are positioned in this region, which indicates the reduction of the NDI moiety through anion–π interactions.[24] Thus, **NDI@silica** interacts with fluoride anions at the solid/liquid interface, analogous to the solution media.

Based on anion–π interactions, the anion species were adsorbed on **NDI@silica**. For quantitative evaluation, the adsorption amounts of the anion species were measured using QCM-D, which can assume the adsorbed mass (Sauerbrey mass, Δm [ng]) owing to changes in the frequency of the QCM-D sensor (ΔF_n [Hz]) by using the following equation: $\Delta m = -C \times (\Delta F_n/n)$, where C is a constant (0.177 mg m^{-2} Hz^{-1}) and n is the overtone number (3 in this study). Pure water was flowed onto the QCM-D silica sensor, modified with **TEG-NDI-TES**, and then, the aqueous solution of TBACl was continuously injected, which resulted in a decrease in ΔF_3, as shown in Fig. 3a. We used a low concentration of TBA salts to exclude the effect of the energy dissipation on the frequency F_n owing to the viscosity and density changes in the bulk solution.

We also examined the adsorption behaviour of **NDI@silica** with several anions (Fig. S5, ESI†). Table 1 shows the frequency change ($\Delta F_3/3$) caused by the flow of anion species and the assumed adsorption amounts of the anions (Γ_{anion} [mol cm^{-2}]). The strength of anion–π interactions depends on the electron density of the anions,[15] which corresponds to their hydration

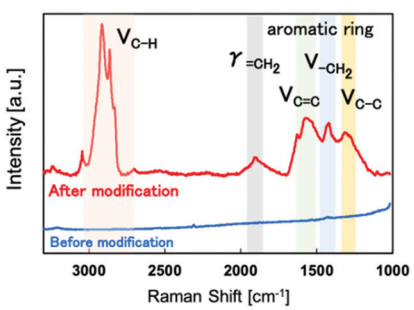

Fig. 2 Raman spectra of **NDI@silica** and bare silica substrate.

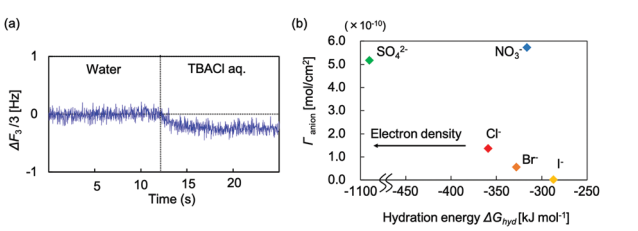

Fig. 3 (a) Variation in the frequency ($\Delta F_3/3$) as a function of time. TBACl concentration was fixed at 1.0×10^{-5} M. (b) Plots of the adsorption amount of the anions (Γ_{anion}) *vs.* the hydration energy of anion species (ΔG_{hyd}).

Table 1 Frequency changes ($\Delta F_3/3$) and adsorption amounts of the anions (Γ_{anion}), ratio of adsorbed anions against one NDI unit on the silica substrate

	NO_3^-	SO_4^{2-}	Cl^-	Br^-	I^-
$\Delta F_3/3$ (Hz)	2.00	2.85	0.27	0.25	N.D.
Γ_{anion} (10^{-10}·mol cm^{-2})	5.71	5.16	1.35	0.55	N.D.
Anion/NDI	0.93	0.84	0.22	0.09	N.D.

energy (ΔG_{hyd}). As shown in Fig. 3b, the plots of Γ_{anion} *vs.* ΔG_{hyd} revealed that halide anions ($Cl^- > Br^- > I^-$) and SO_4^{2-}, and the anions with larger ΔG_{hyd} showed larger adsorption amounts. On the other hand, NO_3^- specifically showed a larger Γ_{anion}. A previous report has presented similar results in that anions with a π-conjugated system show better anion binding with the NDI units than halide anions because of the concerted effect of π–π interaction with anion–π interaction.[15] Furthermore, with anions showing better binding, the frequency change ($\Delta F_3/3$) reached the stationary state more quickly, indicating that the adsorption speed also depends on the strength of anion–π interaction (Fig. S5, ESI†). After replacement with pure water, $\Delta F_3/3$ recovered to the initial value, which also revealed that the anion adsorption is based on a noncovalent interaction (Fig. S5f, ESI†). From these results, we observed the trend of anion adsorption on the NDI-modified substrate, which follows the strengths of anion–π interaction.

Next, to investigate anion–π interactions at the solid/liquid interface, we recorded force curve measurements with AFM, which can measure the physical forces between **NDI@silica** and a silicon nitride cantilever in aqueous media. The surface of the cantilever is negatively charged in water under neutral conditions because the pK_a of silicon nitride is ~5.5.[25,26] Fig. 4a shows a typical force curve of **NDI@silica** with a negatively charged cantilever in pure water. From apparent separation of 3–4 nm, an attractive force of ~0.1 nN was observed. The curve was apparently different from the theoretical curve of the van der Waals attractive force[27] with the assumption of a general organic thin film. In contrast, the TEG-modified silica substrate (**TEG@silica**) showed a repulsive force with respect to the molecular length, which revealed that the attractive force was derived from the NDI moiety (Fig. 4b). The TEG groups on **NDI@silica** can also show similar repulsive force according to the steric effect. One possibility is that the NDI core tilts on the surface owing to interactions of the polar groups of the NDI core and TEG group with the silica surface, and the TEG group located near the surface provides the steric effect in the vicinity of the surface. Therefore, it is expected that anion–π interactions between the NDI-modified substrate and the negative charge are observed in the measurement.

Furthermore, to clarify the anion–π interactions at the interface, we examined the effect of the presence of chloride anions. Based on the Derjaguin–Landau–Verwey–Overbeek (DLVO) theory, the repulsive force was suppressed in the presence of salts owing to the electrostatic shielding on the interfaces and the net attractive force in the presence of salts and can be enhanced compared to that in the absence. However, if the attractive force is derived from the interaction between **NDI@silica** and the cantilever surface, the excess amount of added chloride anions is likely to interact with the NDI moieties on the surface and inhibit the attractive force, resulting in a repulsive force owing to electrostatic repulsion. As a result, repulsive force was observed and then was jumped into attractive force in the presence of 10 mM TBACl. This revealed that an electrostatic repulsive force was cancelled when the negatively charged cantilever entered the NDI film (Fig. 4c). To observe the clear trend of this inhabitation behaviour of the added chloride anion, a histogram of the detected force was created, which confirmed that the attractive force gradually reverted to the repulsive force with increasing chloride ion concentration (Fig. 5a and b and Fig. S6, ESI†). These results revealed that

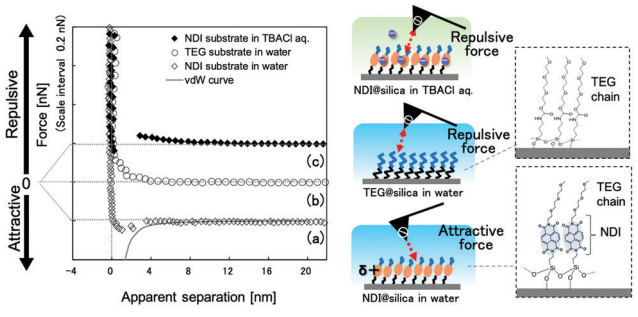

Fig. 4 Approaching force curves of **NDI@silica** in pure water (a), **TEG@silica** substrate in pure water (b), and **NDI@silica** in 10 mM TBACl of aqueous solution (c). The theoretical curve of van der Waals force is attached on the curve of **NDI@silica** in pure water. The *Z*-scale interval is 0.2 nN.

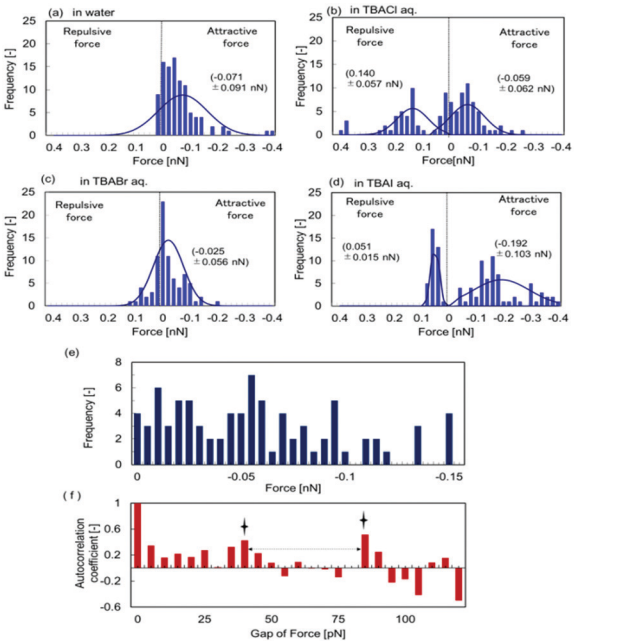

Fig. 5 Histograms of the observed force on **NDI@silica** in pure water (a), aqueous solutions of TBACl (b), TBABr (c), and TBAI (d) (n = 100). The salt concentration was fixed at 10 mM. Detailed histogram of the observed attractive force on **NDI@silica** in pure water (e) and its autocorrelation coefficient (f).

anion–π interactions were observed on **NDI@silica**. This is a remarkable result of direct observation of anion–π interactions with the force measurement, as reported by Zeng.[22] The effect of anion species on the inhibition was examined using 10 mM TBACl, TBABr, and TBAI in water (Fig. 5b–d). According to these histograms, the inhibition behaviour trend was $Cl^- > Br^- > I^-$, which corresponds to the trend of the adsorption amount obtained by the QCM-D measurements and a previous report.[15] The results of this study show that the stronger the anion–π interaction between **NDI@silica** and the species, the greater the amount of anion adsorption, resulting in a higher probability of repulsive force. Finally, by using autocorrelation function analysis,[28] we assumed a single-molecule force of anion–π interaction at the interface. Fig. 5f shows the autocorrelation coefficient according to the detailed histogram of the attractive force observed on **NDI@silica** in pure water (Fig. 5e). This revealed the peak periodicity of the interval of ~40 pN, which represents the single-molecule force of anion–π interaction observed here. The single-molecule of anion–π interaction is comparable with those of other molecular interactions, such as cation–π interactions with calixarene–ammonium cations (~80 pN)[29] and the strong antigen–antibody interaction with avidin–biotin (160 pN),[30] suggesting that the obtained value of the single-molecule force is sufficient for the interaction. To the best of our knowledge, this is the first example of obtaining a single-molecule force for anion–π interactions.

In conclusion, we evaluated anion–π interactions at the solid/aqueous solution interface by using films based on the NDI analogue that is a popular and simple anion–π acceptor. The strength of the interaction followed the trend $NO_3^- > SO_4^{2-} > Cl^- > Br^- > I^-$, as revealed by adsorption measurements by QCM-D and inhabitation experiments on the force curve measurements, which corresponds to the extent of the hydration energy and the presence of the conjugated systems of the anions. The force curve measurements demonstrated direct observation of anion–π interactions, and autocorrelation analysis revealed the single-molecule force to be ~40 pN. Based on this finding, we are currently working on controlling the macroscopic physical properties of the solid/water interface, such as wettability and particle dispersibility, using anion-specific and selective adsorption of anions. We hope that the results obtained in this study will lead to the development of various functional materials and stimulus-responsive materials in the future.

This work was supported by the Foundation, Oil & Fat Industry Kaikan.

Conflicts of interest

There are no conflicts to declare.

Notes and references

1 M. Giese, M. Albrecht and K. Rissanen, *Chem. Commun.*, 2015, **52**, 1778–1795.
2 D. Y. Sasaki, K. Kurihara and T. Kunitake, *J. Am. Chem. Soc.*, 1992, **114**, 10994–10995.
3 M. Onda, K. Yoshihara, H. Koyano, K. Ariga and T. Kunitake, *J. Am. Chem. Soc.*, 1996, **118**, 8524–8530.
4 K. Ariga and T. Kunitake, *Acc. Chem. Res.*, 1998, **31**, 371–378.
5 L. Fumagalli, A. Esfandiar, R. Fabregas, S. Hu, P. Ares, A. Janardanan, Q. Yang, B. Radha, T. Taniguchi, K. Watanabe, G. Gomila, K. S. Novoselov and A. K. Geim, *Science*, 2018, **360**, 1339–1342.
6 H. T. Chifotides and K. R. Dunbar, *Acc. Chem. Res.*, 2013, **46**, 894–906.
7 D. A. Dougherty, *Acc. Chem. Res.*, 2013, **46**, 885–893.
8 B. L. Schottel, H. T. Chifotides and K. R. Dunbar, *Chem. Soc. Rev.*, 2008, **37**, 68–83.
9 P. Gamez, T. J. Mooibroek, S. J. Teat and J. A. N. Reedijk, *Acc. Chem. Res.*, 2007, **40**, 435–444.
10 O. B. Berryman, F. Hof, M. J. Hynes and D. W. Johnson, *Chem. Commun.*, 2006, 506–508.
11 D. X. Wang, Q. Q. Wang, Y. Han, Y. Wang, Z. T. Huang and M. X. Wang, *Chem. – Eur. J.*, 2010, **16**, 13053–13057.
12 Y. Zhao, Y. Cotelle, L. Liu, J. López-López-Andarias, A.-B. Bornhof, M. Akamatsu, N. Sakai and S. Matile, *Acc. Chem. Res.*, 2018, **51**, 2255–2263.
13 I. A. Rather, S. A. Wagay and R. Ali, *Coord. Chem. Rev.*, 2020, **415**, 213327.
14 D. X. Wang and M. X. Wang, *Acc. Chem. Res.*, 2020, **53**, 1364–1380.
15 R. E. Dawson, A. Hennig, D. P. Weimann, D. Emery, V. Ravikumar, J. Montenegro, T. Takeuchi, S. Gabutti, M. Mayor, J. Mareda, C. A. Schalley and S. Matile, *Nat. Chem.*, 2010, **2**, 533–538.
16 M. Akamatsu, N. Sakai and S. Matile, *J. Am. Chem. Soc.*, 2017, **139**, 6558–6561.
17 C. Estarellas, A. Frontera, D. Quiñonero and P. M. Deyã, *Angew. Chem., Int. Ed.*, 2011, **50**, 415–418.
18 X. Lucas, A. Bauzá, A. Frontera and D. Quiñonero, *Chem. Sci.*, 2016, **7**, 1038–1050.
19 J. Zhang, L. Xiang, B. Yan and H. Zeng, *J. Am. Chem. Soc.*, 2020, **142**, 1710–1714.
20 T. Auletta, M. R. De Jong, A. Mulder, F. C. J. M. Van Veggel, J. Huskens, D. N. Reinhoudt, S. Zou, S. Zapotoczny, H. Schönherr, G. J. Vancso and L. Kuipers, *J. Am. Chem. Soc.*, 2004, **126**, 1577–1584.
21 M. A. Gebbie, W. Wei, A. M. Schrader, T. Cristiani, J. H. Waite and N. Israelachvili, *Nat. Chem.*, 2017, **9**, 473–479.
22 J. Zhang, L. Xiang, B. Yan and H. Zeng, *J. Am. Chem. Soc.*, 2020, **142**, 1710–1714.
23 S. Guha and S. Saha, *J. Am. Chem. Soc.*, 2010, **132**, 17674–17677.
24 G. Aragay, A. Frontera, V. Lloveras, J. Vidal-Gancedo and P. Ballester, *J. Am. Chem. Soc.*, 2013, **135**, 2620–2627.
25 B. Zhu, P. Xia, W. Ho and J. Yu, *Appl. Surf. Sci.*, 2015, **344**, 188–195.
26 E. P. Luther, T. M. Kramer, F. F. Lange and D. S. Pearson, *J. Am. Ceram. Soc.*, 1994, **77**, 1047–1051.
27 J. N. Israelachvili, *Intermolecular and Surface Forces*, Academic Press, London, 3rd edn, 2011.
28 H. Schönherr, M. W. J. Beulen, J. Bügler, J. Huskens, F. C. J. M. Van Veggel, D. N. Reinhoudt and G. J. Vancso, *J. Am. Chem. Soc.*, 2000, **122**, 4963–4967.
29 R. Eckel, R. Ros, B. Decker, J. Mattay and D. Anselmetti, *Angew. Chem., Int. Ed.*, 2005, **44**, 484–488.
30 E. Florin, V. T. Moy and H. E. Gaub, *Science*, 1994, **264**, 415–418.